

TAT
W34m
No. S-78-15
Cop. 2



US-CE-C Property of the United States Government



MISCELLANEOUS PAPER S-78-15

SUMMARY OF NUMERICAL ANALYSES OF THE EFFECT OF W/A IN EARTH PENETRATION

by

Mark H. Wagner, Christopher C. Fulton
California Research and Technology, Inc.
6269 Variel Avenue, Suite 200
Woodland Hills, Calif. 91367

September 1978
Final Report

Approved For Public Release; Distribution Unlimited



Prepared for Office, Chief of Engineers, U. S. Army
Washington, D. C. 20314

Under Project 4A16II02AT22, Task A2, Work Unit 006

Monitored by Soils and Pavements Laboratory
U. S. Army Engineer Waterways Experiment Station
P. O. Box 631, Vicksburg, Miss. 39180

LIBRARY BRANCH
TECHNICAL INFORMATION CENTER
U.S. ARMY ENGINEER WATERWAYS EXPERIMENT STATION
VICKSBURG, MISSISSIPPI

Unclassified

SECURITY CLASSIFICATION OF THIS PAGE (When Data Entered)

20. ABSTRACT (Continued).

the U. S. Army Engineer Waterways Experiment Station.

The penetrator problems consisted of the normal impacts of rigid-body projectiles into sand targets at a velocity of 200 ft/sec. The projectiles for Cases 1 and 2 were 6 in. in diameter with a 6-in.-long ogive nose ($CRH = 1.25$). The Case 3 projectile was scaled up in size by $\sqrt{3}$, giving a 10.392-in.- by 10.392-in.-diameter nose. Two penetrator weights were selected, 141.4 lb (Case 1) and 424.1 lb (Cases 2 and 3), to give projectile sectional pressures of 5 psi for Cases 1 and 3 and 15 psi for Case 2.

The solutions of each penetrator problem were run from initial impact to a penetration depth of 1-1/3 nose lengths. The computed penetration dynamics indicated that the comparative penetrator decelerations were related to the sectional pressure by $a^\alpha(W/A)^{-1}$, in agreement with conventional (rate-independent) scaling rules. During the later stages of the penetrations, the relative decelerations tended to depart from this rule. These deviations are believed to be due principally to the effects of the nonequivalent projectile velocities that developed during the penetrations, resulting from the different deceleration levels or event durations associated with each case.

Since there is some experimental evidence suggesting that penetrator decelerations of this type are related by $a^\alpha(W/A)^{-1/2}$, there is the possibility that rate-dependent behavior, such as viscoplasticity, may be occurring in the media that should be accounted for in the material models.

Detailed results of the numerical analyses, including time histories of the penetration dynamics variables, force loading distributions, and field plots of the target response, are presented.

PREFACE

This report was prepared by Messrs. Mark H. Wagner and Christopher C. Fulton of California Research and Technology, Inc., Woodland Hills, California, under Purchase Order DACA39-78-M-0030 as a part of ongoing work at the U. S. Army Engineer Waterways Experiment Station (WES), DA Project No. 4A161102AT22, Task A2, Work Unit 006, "Effectiveness of Earth Penetrators in Various Geologic Environments." The principal investigator at California Research and Technology was Mr. Wagner. The programming and computer runs were conducted by Mr. Fulton.

The problems were specified and the work was monitored by Dr. Behzad Rohani of the Soil Dynamics Division (SDD), Soils and Pavements Laboratory (S&PL), WES, under the supervision of Dr. J. G. Jackson, Jr., Chief, SDD, and the general direction of Mr. James P. Sale, Chief of S&PL.

COL J. L. Cannon, CE, was Commander and Director of WES during the preparation and publication of this report. Mr. F. R. Brown was Technical Director.

CONTENTS

	<u>Page</u>
PREFACE	1
CONVERSION FACTORS, U. S. CUSTOMARY TO METRIC (SI)	
UNITS OF MEASUREMENT	3
SCOPE	4
DESCRIPTION OF PENETRATOR PROBLEMS	4
COMPUTATIONAL METHOD	5
NUMERICAL SOLUTION RESULTS	5
REFERENCES	7
TABLES 1 AND 2	
FIGURES 1-19	

CONVERSION FACTORS, U. S. CUSTOMARY TO METRIC (SI)
UNITS OF MEASUREMENT

U. S. customary units of measurement used in this report can be converted to metric (SI) units as follows:

<u>Multiply</u>	<u>By</u>	<u>To Obtain</u>
feet per second	0.3048	metres per second
inches	0.0254	metres
kips (force)	4448.222	newtons
pounds (force) per square inch	6.894757	kilopascals

SUMMARY OF NUMERICAL ANALYSES OF THE
EFFECT OF W/A IN EARTH PENETRATION

1. SCOPE

This report describes the results of a finite-difference code calculation of projectile penetration conducted by California Research and Technology, Inc., to provide information of use in the study of penetrator scaling relations. This calculation was for the third case in a series of three penetration analyses. Pertinent results from the analyses of the first two cases¹ are included herein for comparative purposes.

2. DESCRIPTION OF PENETRATOR PROBLEMS

The penetrator problem considered was the normal impact of a rigid-body projectile into a sand target at 200 ft/sec,* as shown in Figure 1. This problem was designated Case 3 in a series of three penetration computations. The conditions for all three cases are listed in Table 1. Cases 1 and 2 have the same projectile nose geometry, with the total projectile weight, or W/A, of Case 2 being three times greater than for Case 1. The Case 3 projectile nose geometry is scaled up by a factor of $\sqrt{3}$ over that of the Case 1 projectile, but retains the same sectional pressure, $W/A = 5$ psi. The impact velocity, nose shape, and target medium were the same in all three cases.

The nominal properties of the sand target are listed in Table 2. The material model used was the same as that used for Layer 2 of the Watchung Hill Site at Defence Research Establishment Suffield in a previous study,² except that the low-pressure end of the yield surface was modified so that the cohesion would be equal to zero.

The penetrator/target interface was assumed to be frictionless for these problems.

* A table of factors for converting U. S. customary units of measurement to metric (SI) units is found on page 3.

3. COMPUTATIONAL METHOD

The numerical solutions of these penetrator problems were obtained with WAVE-L, a two-dimensional finite-difference Lagrangian hydrodynamic-elastic-plastic code. This code has been employed to solve penetrator problems on a number of Defense Nuclear Agency and U. S. Army Engineer Waterways Experiment Station projects during the past few years.

The computational grid setup for the Case 3 problem is partially shown in Figure 2. The basic cell size used in the target was $\Delta r_0 = \Delta z_0 = 0.866$ in., or 1/6 the projectile radius. Beyond a radius of 10.4 in. and a depth of 20.8 in., the cell dimensions were gradually increased in 2 percent steps. The overall grid extended to a radius of 52.8 in. and a depth of 63.2 in., comprising 2800 grid points. This grid extends beyond the boundaries of wave propagation that took place during the problem (which was run to a penetration depth of ~ 14 in.) so that it could be restarted and continued to longer times if desired.

The integration time step varies during the course of the problem, depending on the sound speed, minimum cell dimension, and stability criteria selected. For this problem, the average time step was 2.7 μ sec.

4. NUMERICAL SOLUTION RESULTS

Each of the three penetrator problems was run from initial impact to a penetration depth of 1-1/3 nose lengths, i.e., penetration depths of 8 in. for Cases 1 and 2 and 13.9 in. for Case 3. The computed penetrator deceleration versus depth of penetration for each case is shown in Figure 3. Time histories of the penetrator deceleration, velocity, depth of penetration, and attached length (vertical distance from nose tip to point of separation of projectile from target) are shown in Figure 4. The deceleration for Case 1 is seen to be approximately three times that of Case 2, i.e., the decelerations are approximately inversely proportional to the penetrator weights (or W/A). Comparing Cases 3 and 1, which have the same W/A, the peak deceleration levels are seen to be about the same, with the deceleration profiles for Case 3 stretched out over a greater penetration depth and time, due to the $\sqrt{3}$ scale-up in size of the projectile nose. Comparisons of the computed

penetrator deceleration and the change in projectile velocity during the penetration on a scaled basis are shown in Figures 5 and 6. Using conventional (rate-independent) scaling relations, the indicated deceleration and velocity change ratios should be equal to a value of 1 for changes in just the weight or area (diameter), i.e., holding all other problem variables constant. The computed results are seen to vary around 1 for Case 3/Case 1. For Case 2/Case 1, the scaled ratios are seen to oscillate around a value of 1 for about the first half of nose embedment; the ratios then steadily increase for the rest of the solution (to a projectile embedment of 1-1/3 nose lengths). The gradually larger decelerating force seen for the heavier Case 2 projectile is believed to be due to a velocity effect. Note in Figure 3 that the Case 2 penetration velocity is higher relative to Case 1, with the gap increasing, due to its substantially lower deceleration level. The relative velocities, plotted versus penetration depth/nose length, are shown in Figure 7. For Case 3/Case 1, the deceleration levels are comparable, but the event time is scaled up for the larger diameter Case 3 projectile, so that the relative velocity, $v_{\text{Case 3}}/v_{\text{Case 1}}$, is decreasing. This may account for the downward trend in the deceleration ratio, $a_{\text{Case 3}}/a_{\text{Case 1}}$, beyond one nose length.

There is some experimental evidence indicating that the total penetration depth is proportional to $(W/A)^{1/2}$ for low-velocity projectile penetrations into soil.^{3,4} The penetrator decelerations from the analyses conducted herein do not deviate largely from direct inverse proportionality on W/A , i.e., $a \propto (W/A)^{-1}$, which would generally indicate that (for these type penetrations) the total penetration depth would be directly proportional to W/A , i.e., $Z \propto W/A$. The direct proportionality is also what would be predicted from conventional scaling. Conventional scaling, and the material models in the code, presume that rate effects are not significant. The difference in the experimental and computational trends suggests the possibility that rate effects, such as viscoplastic behavior of the soil, may indeed be affecting the dynamics and that they should be included in the material model.

A series of field plots at penetration depths of $2\sqrt{3}$, $4\sqrt{3}$, $6\sqrt{3}$,

and $8\sqrt{3}$ in. were obtained from the Case 3 analysis, as shown in Figures 8 through 15. For comparative purposes, these depths correspond to the same penetration depth/nose length values for which plots of Cases 1 and 2 were obtained, as presented in Reference 1. The field plots show the overall projectile and target configuration, the extent of plastic deformation in terms of the generalized plastic strain (ϵ^P), the velocity vectors, and the principal stress field.

The computed loadings on the projectile, i.e., distributions of normal stress, axial force, and radial force, for the same penetration depths, are shown in Figures 16 through 19.

REFERENCES

1. M. H. Wagner and C. C. Fulton, *Numerical Analyses of Penetration Dynamics in Support of Investigations of Scaling Relations for Earth Penetrators*, U. S. Army Engineer Waterways Experiment Station, Miscellaneous Paper S-77-23, November 1977.
2. M. H. Wagner, K. N. Kreyenhagen, and W. S. Goerke, *Numerical Analysis of DNA Earth Penetrator Experiment at DRES*, DNA Report 3537F, June 1975.
3. C. W. Young, *Depth Prediction for Earth-Penetrating Projectiles*, Journal, Soil Mechanics and Foundation Div., ASCE, 95, 803 (1969).
4. C. W. Young and G. M. Ozanne, *Compilation of Low Velocity Penetration Data*, Sandia Laboratory, Report SC-RR-66-306A, June 1966.

TABLE 1. PENETRATOR PROBLEM CONDITIONS

	Projectile					Target
	Impact Velocity	Weight	Diameter	W/A	Nose (tangent ogive)	
Case 1	200 ft/sec	64.125 kg (141.4 lb)	6 in.	5 psi	1.25 CRH	Sand
Case 2	200 ft/sec	192.375 kg (424.1 lb)	6 in.	15 psi	1.25 CRH	Sand
Case 3	200 ft/sec	192.375 kg (424.1 lb)	10.392 in. ($6\sqrt{3}$ in.)	5 psi	1.25 CRH	Sand

TABLE 2. PROPERTIES OF SAND TARGET

Density, ρ_0	1.4256 gm/cm ³ 89 lb/ft ³
Air fraction, V_a	40%
Cohesion	0
Unconfined compressive strength	0
Unconfined tensile strength	0
Mises limit, $Y_{max} = \sqrt{3}J_2'_{max}$	2906 psi
Initial value of:	
Bulk modulus, K_0	3292 psi
Shear modulus, G_0	2469 psi
Constrained modulus, M'_0	6585 psi
Young's modulus, E_0	5926 psi
Poisson's ratio, ν_0	0.2
Dilatational velocity, c_0	585 ft/sec

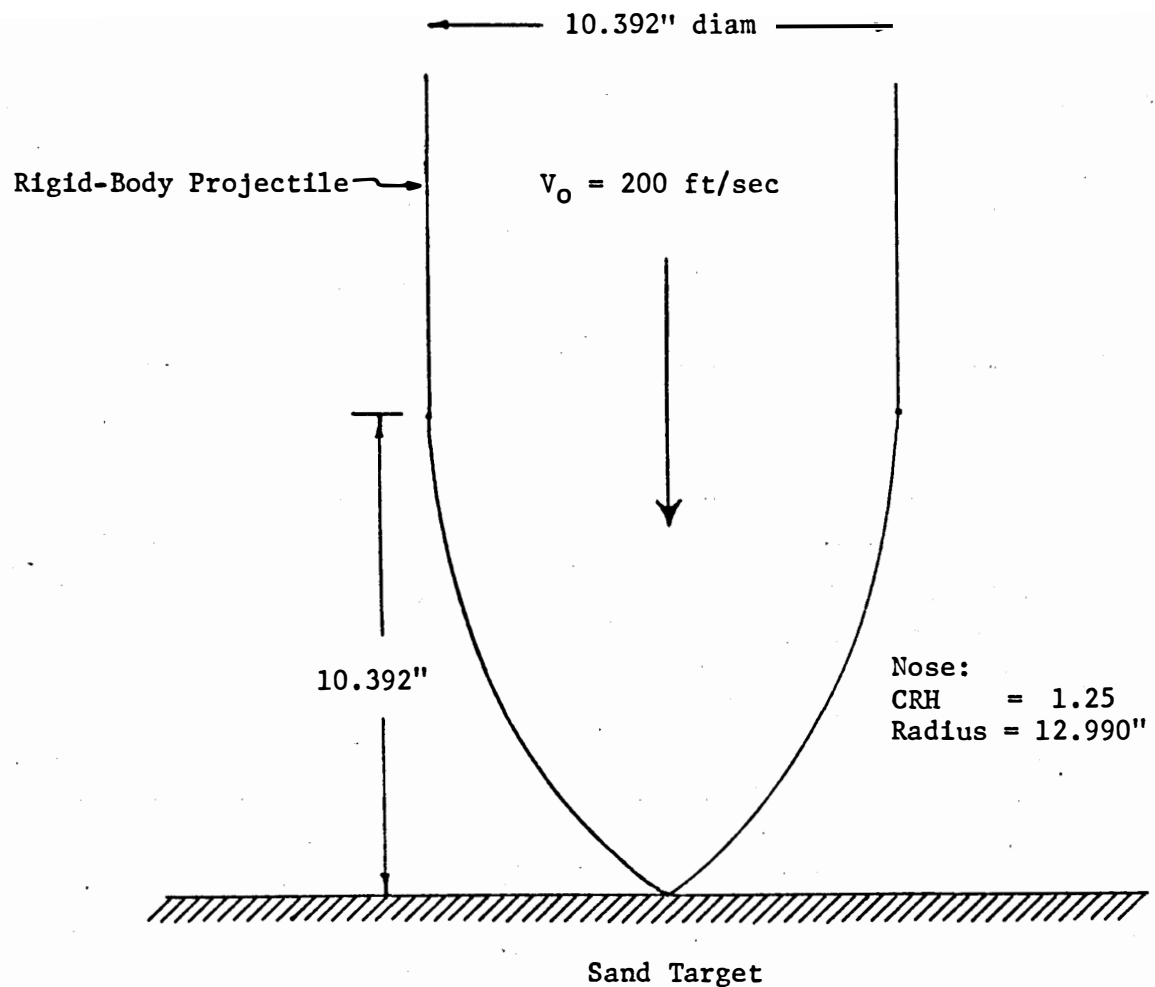


Figure 1. Penetrator Problem Conditions.

CALIFORNIA RESEARCH AND TECHNOLOGY, INC.
RUN NO. 5180-S. LOW VELOCITY PENETRATION CASE S
CYCLE 0

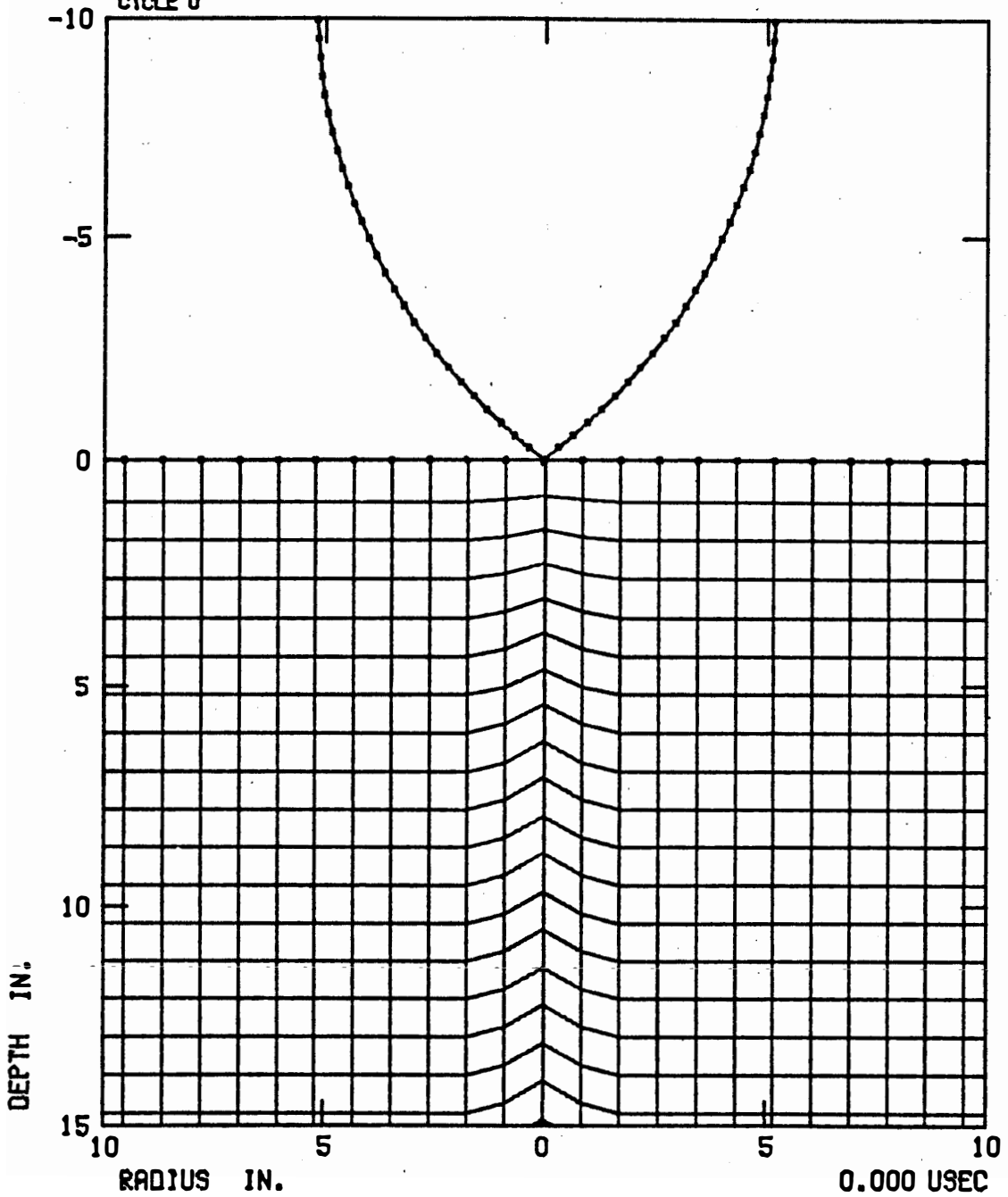


Figure 2. Initial Computational Grid, Case 3.

CALIFORNIA RESEARCH AND TECHNOLOGY, INC.
LOW VELOCITY PENETRATION COMPARISON

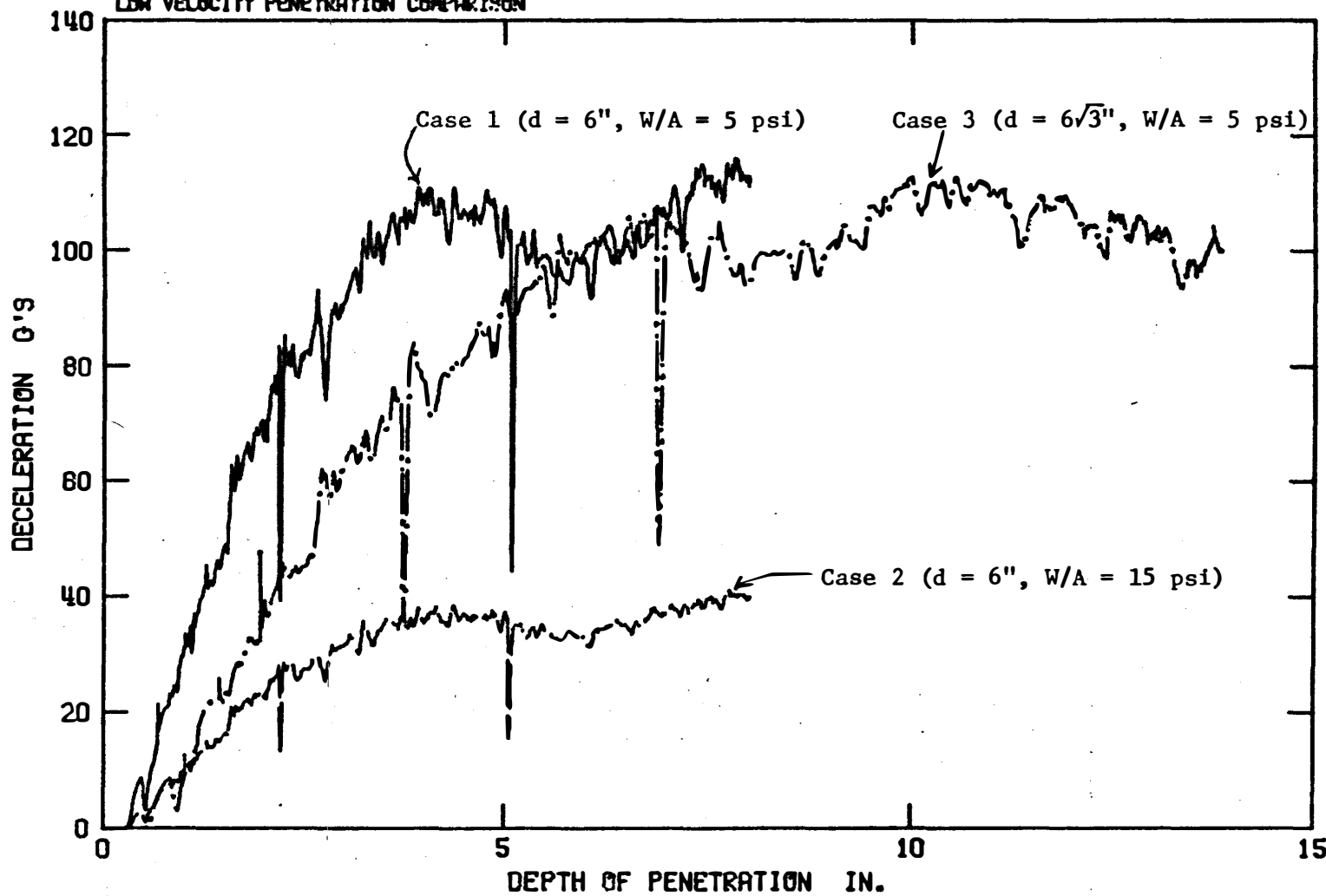


Figure 3. Penetrator Deceleration versus Depth of Penetration.

CALIFORNIA RESEARCH AND TECHNOLOGY, INC.
LOW VELOCITY PENETRATION COMPARISON — PROJECTILE DYNAMICS

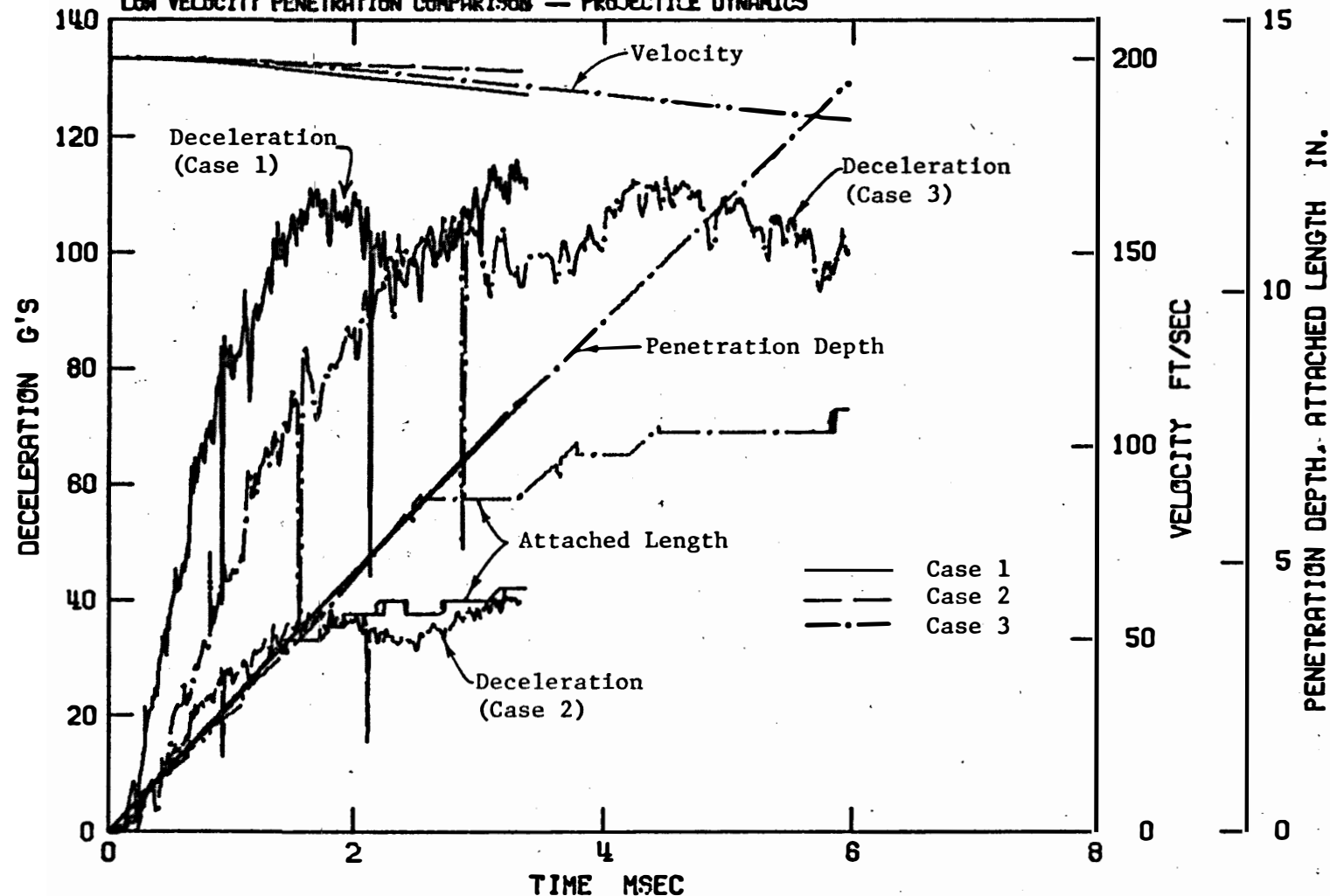


Figure 4. Time Histories of Penetrator Deceleration, Velocity, Depth of Penetration, and Attached Length.

CALIFORNIA RESEARCH AND TECHNOLOGY, INC.
LOW VELOCITY PENETRATION COMPARISONS

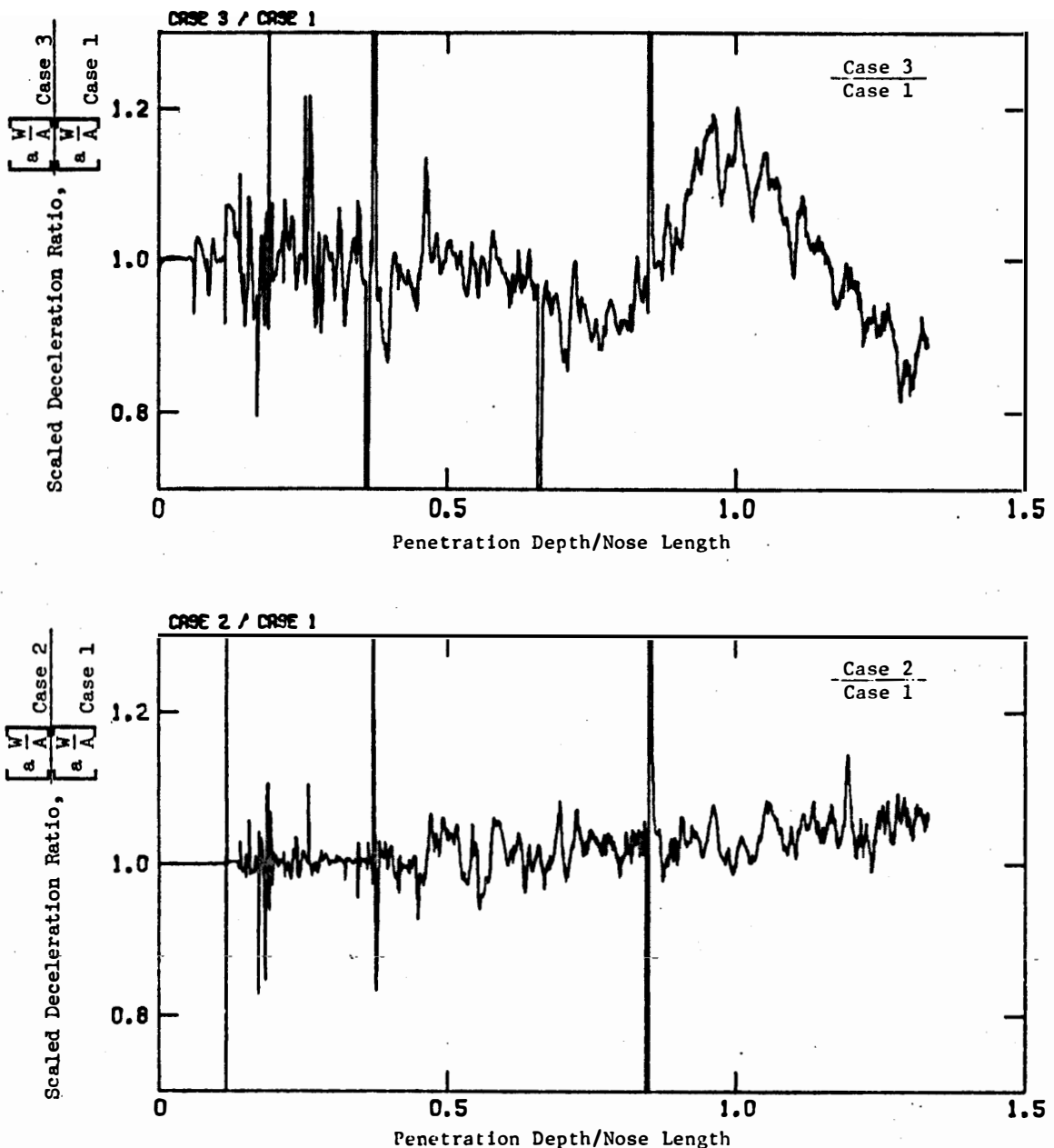


Figure 5. Ratio of Scaled Deceleration versus Penetration Depth/Nose Length.

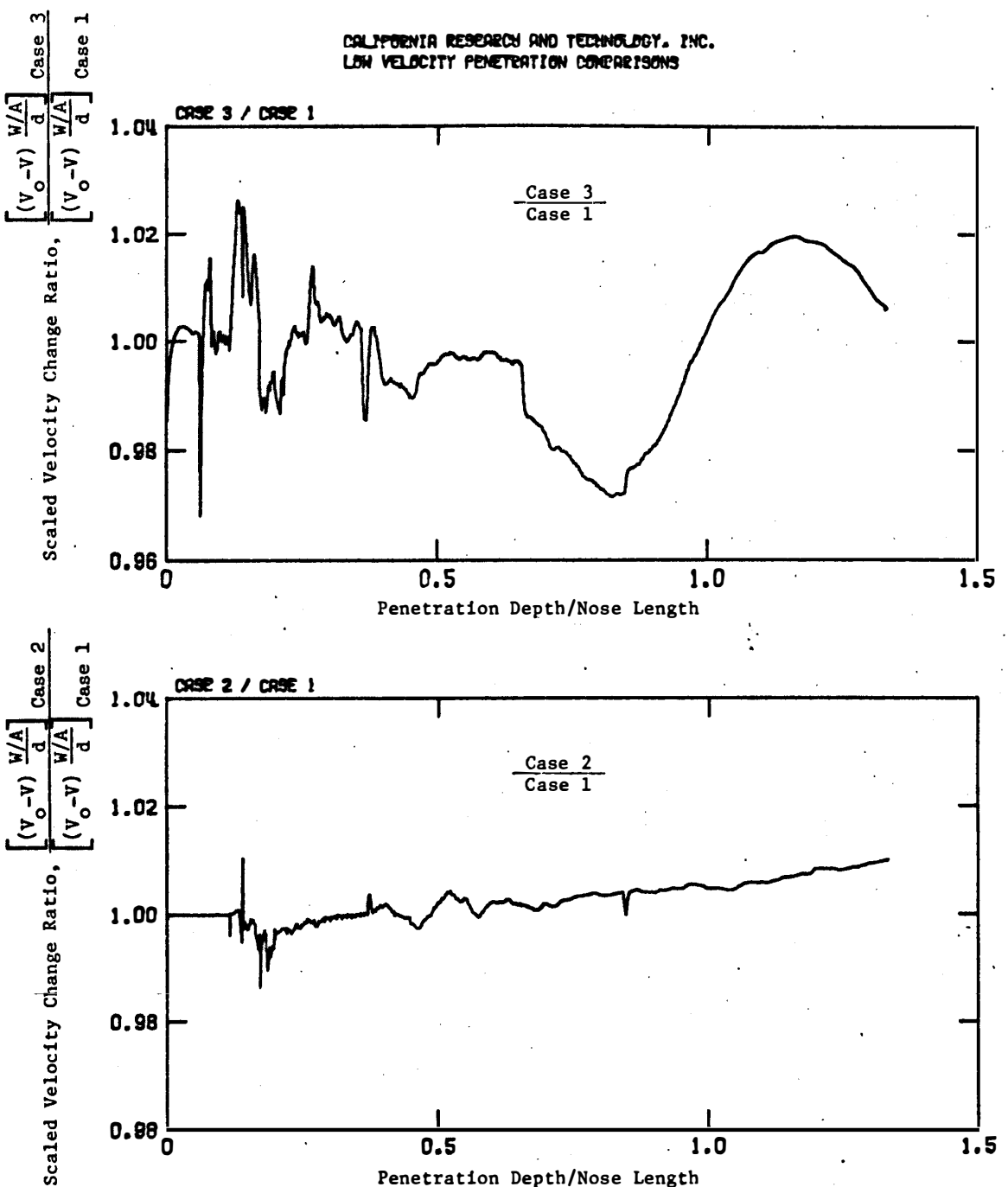


Figure 6. Ratio of Scaled Change in Velocity versus Penetration Depth/Nose Length.

CALIFORNIA RESEARCH AND TECHNOLOGY, INC.
LOW VELOCITY PENETRATION COMPARISONS

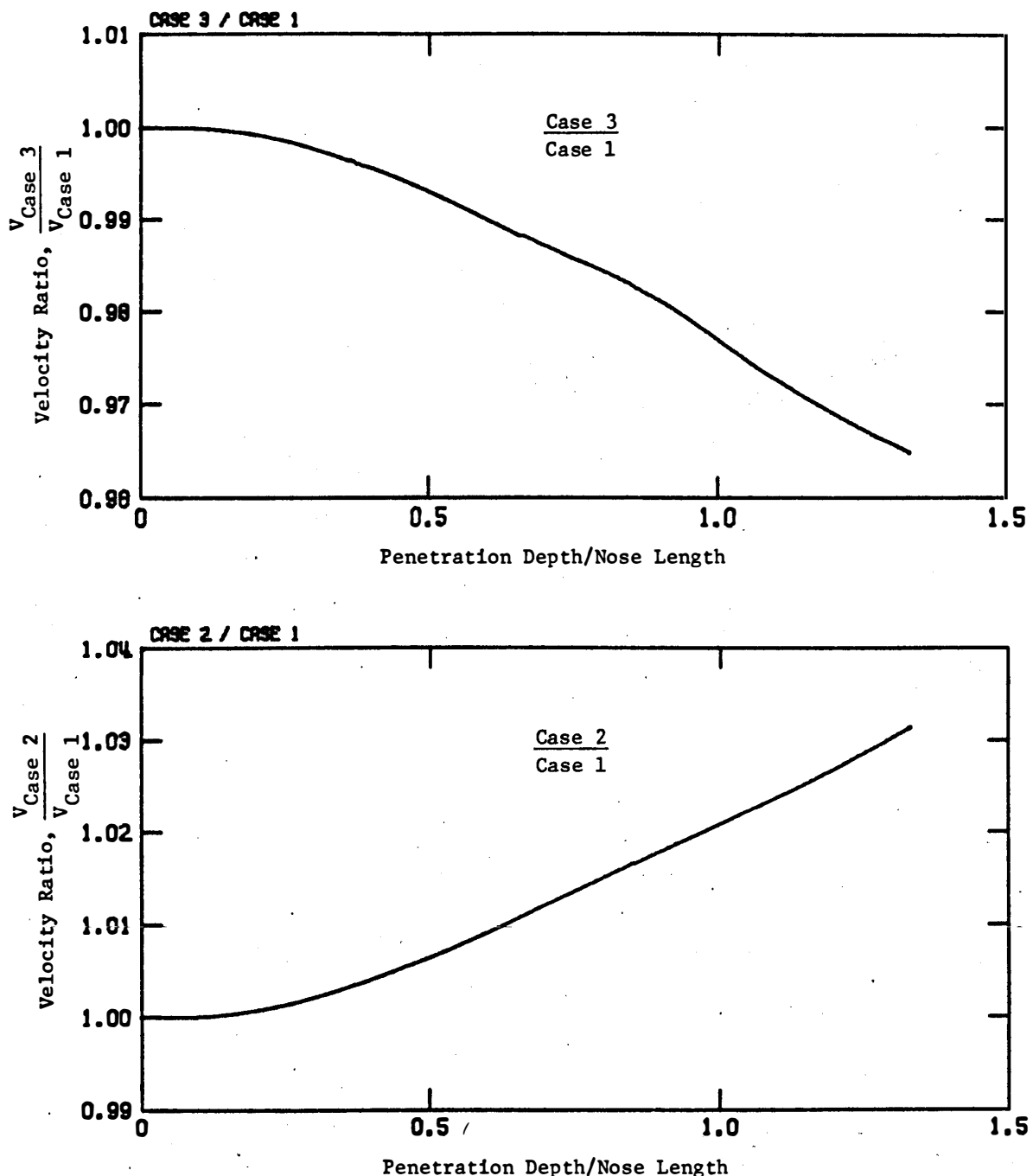


Figure 7. Ratio of Projectile Velocity versus Penetration Depth/Nose Length.

CALIFORNIA RESEARCH AND TECHNOLOGY, INC.
RUN NO. 5180-3, LOW VELOCITY PENETRATION CASE 3
CYCLE 455

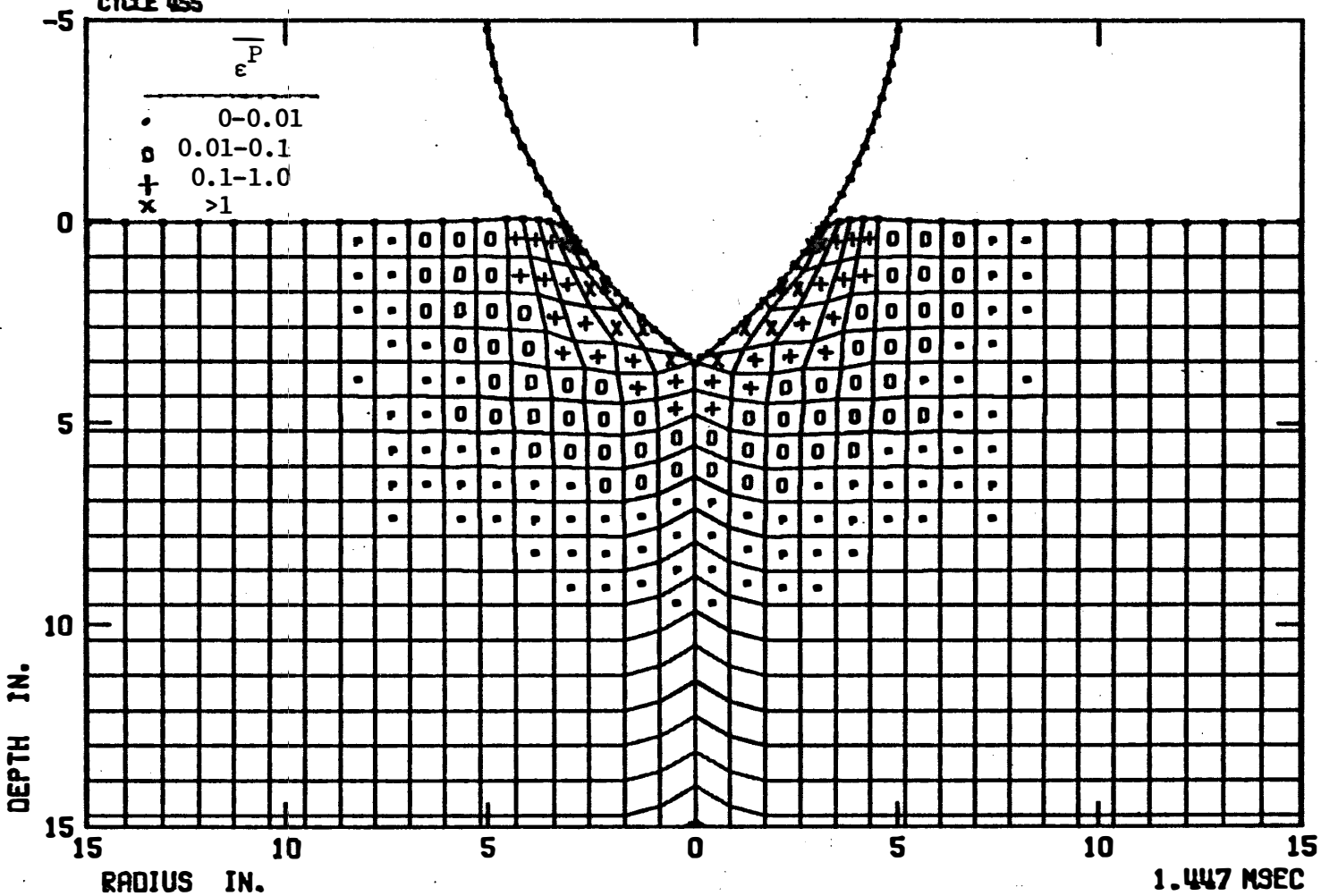


Figure 8. Grid Configuration and Generalized Plastic Strain Field at $2\sqrt{3}$ -in. Penetration Depth, Case 3.

VUNIT= 1.155E-03

SUNIT= 2.909E-05

CALIFORNIA RESEARCH AND TECHNOLOGY, INC.
RUN NO. 5180-3. LOW VELOCITY PENETRATION CASE 3
CYCLE 455 150 FT/SEC

1 0.02 KB

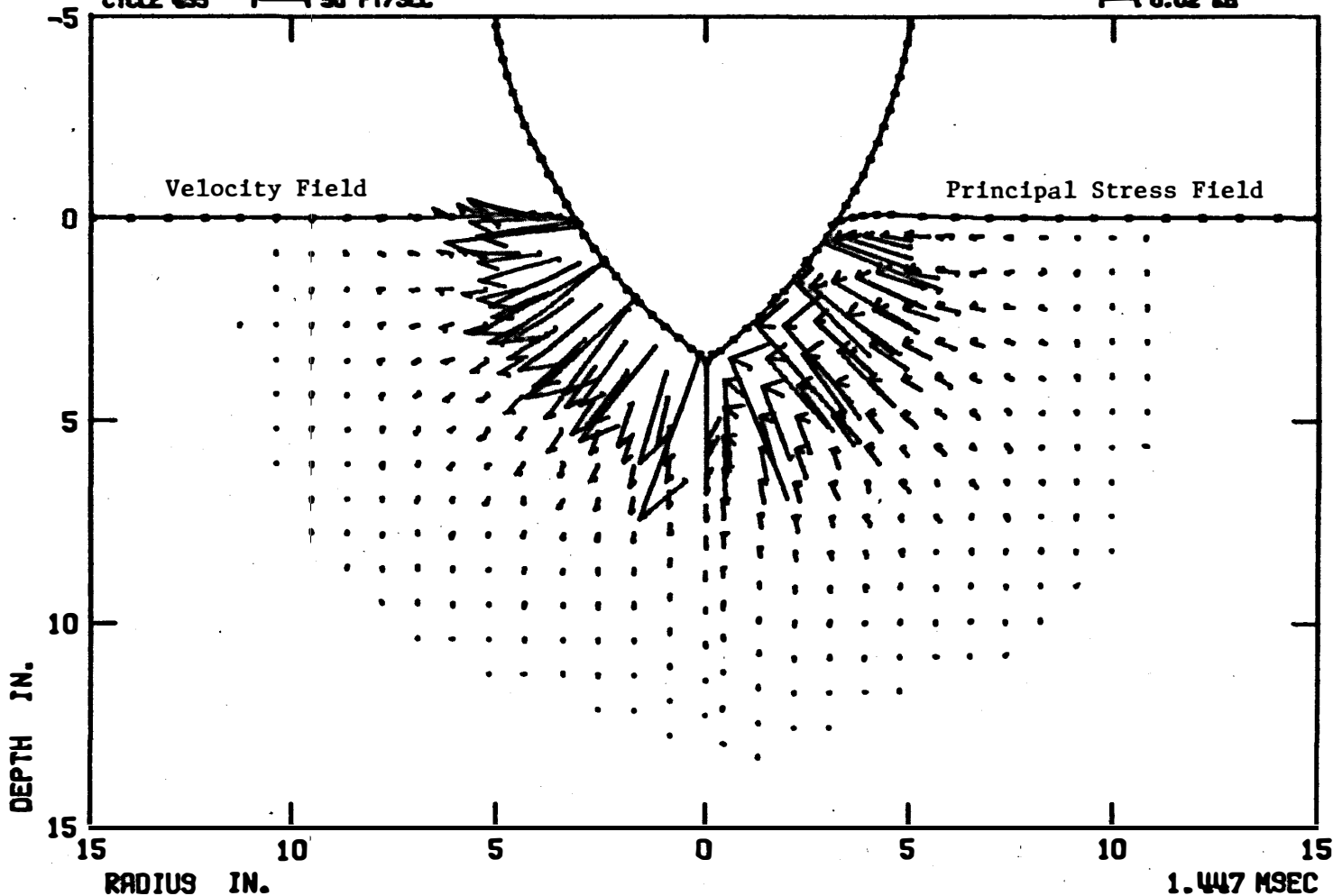


Figure 9. Velocity Field and Principal Stress Field at $2\sqrt{3}$ -in. Penetration Depth, Case 3.

CALIFORNIA RESEARCH AND TECHNOLOGY, INC.
RUN NO. S180-3, LOW VELOCITY PENETRATION CASE 3
CYCLE 1084

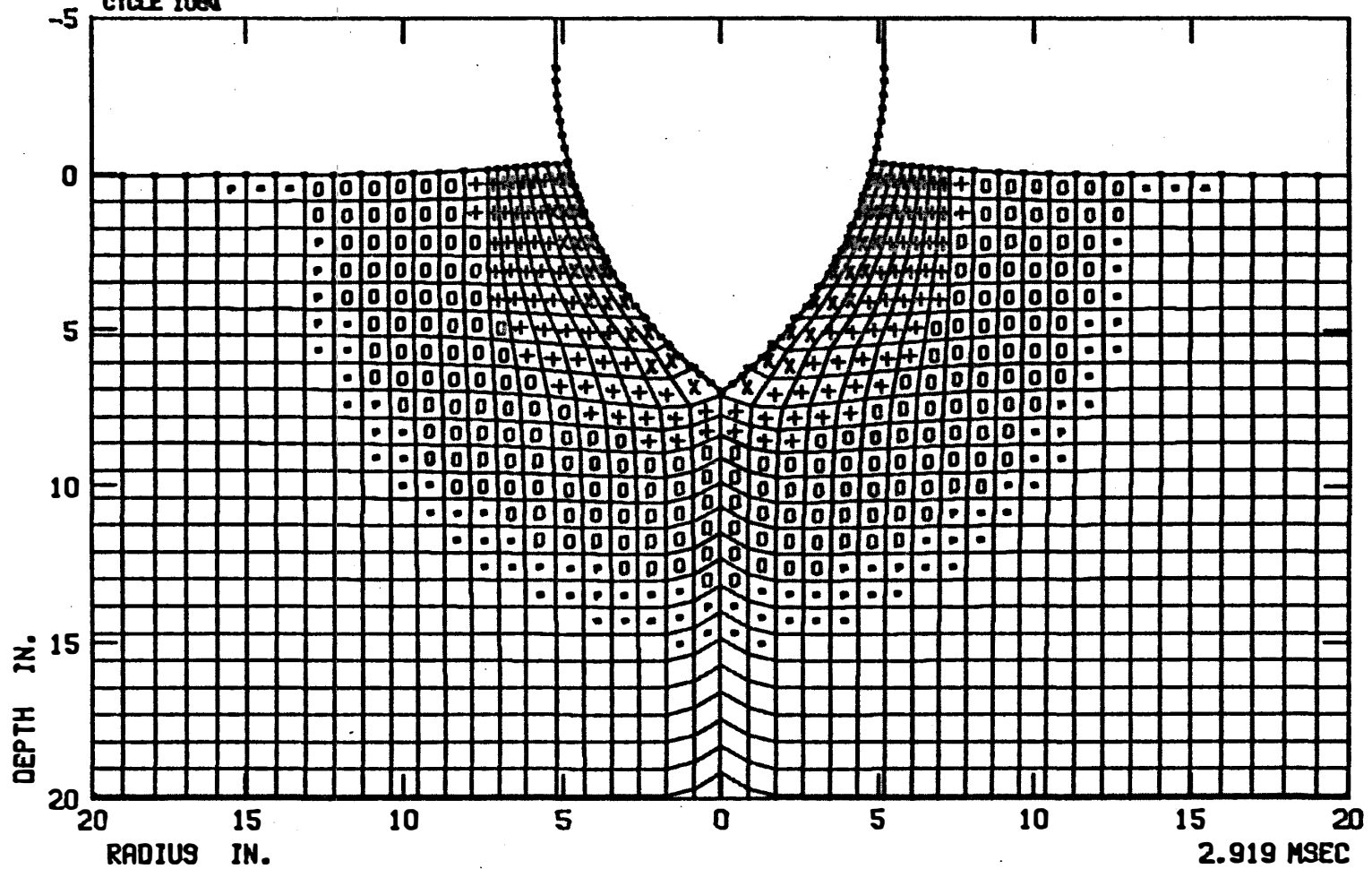


Figure 10. Grid Configuration and Generalized Plastic Strain Field at $4\sqrt{3}$ -in. Penetration Depth, Case 3.

VUNIT= 1.155E-09

SUNIT= 2.309E-05

CALIFORNIA RESEARCH AND TECHNOLOGY, INC.
RUN NO. 5180-3, LOW VELOCITY PENETRATION CASE 3
CYCLE 1084 $\frac{1}{4}$ 50 FT/SEC

1 0.05 KB

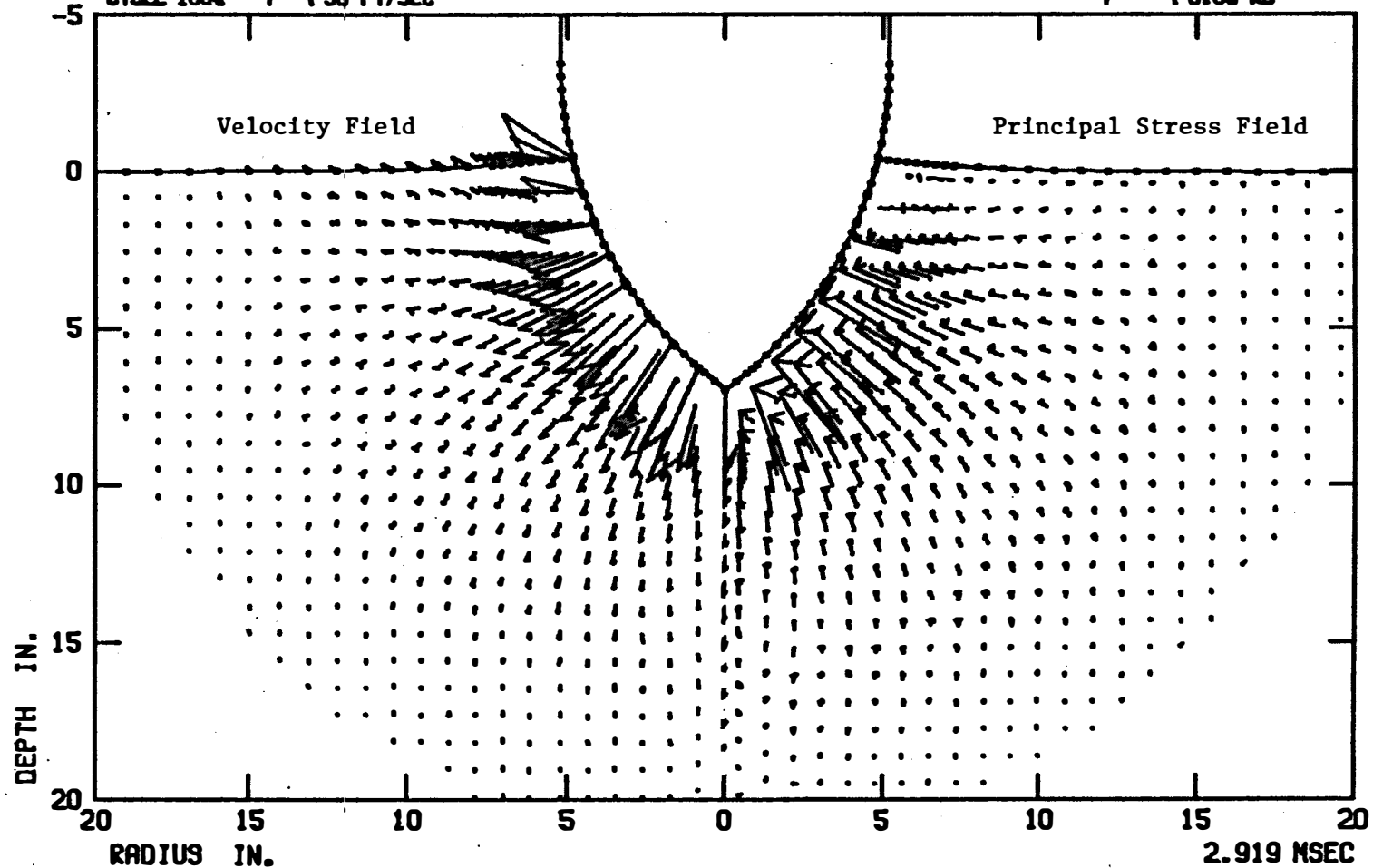


Figure 11. Velocity Field and Principal Stress Field
at $4\sqrt{3}$ -in. Penetration Depth, Case 3.

CALIFORNIA RESEARCH AND TECHNOLOGY, INC.
RUN NO. 5160-3, LOW VELOCITY PENETRATION CASE 3
CYCLE 1453

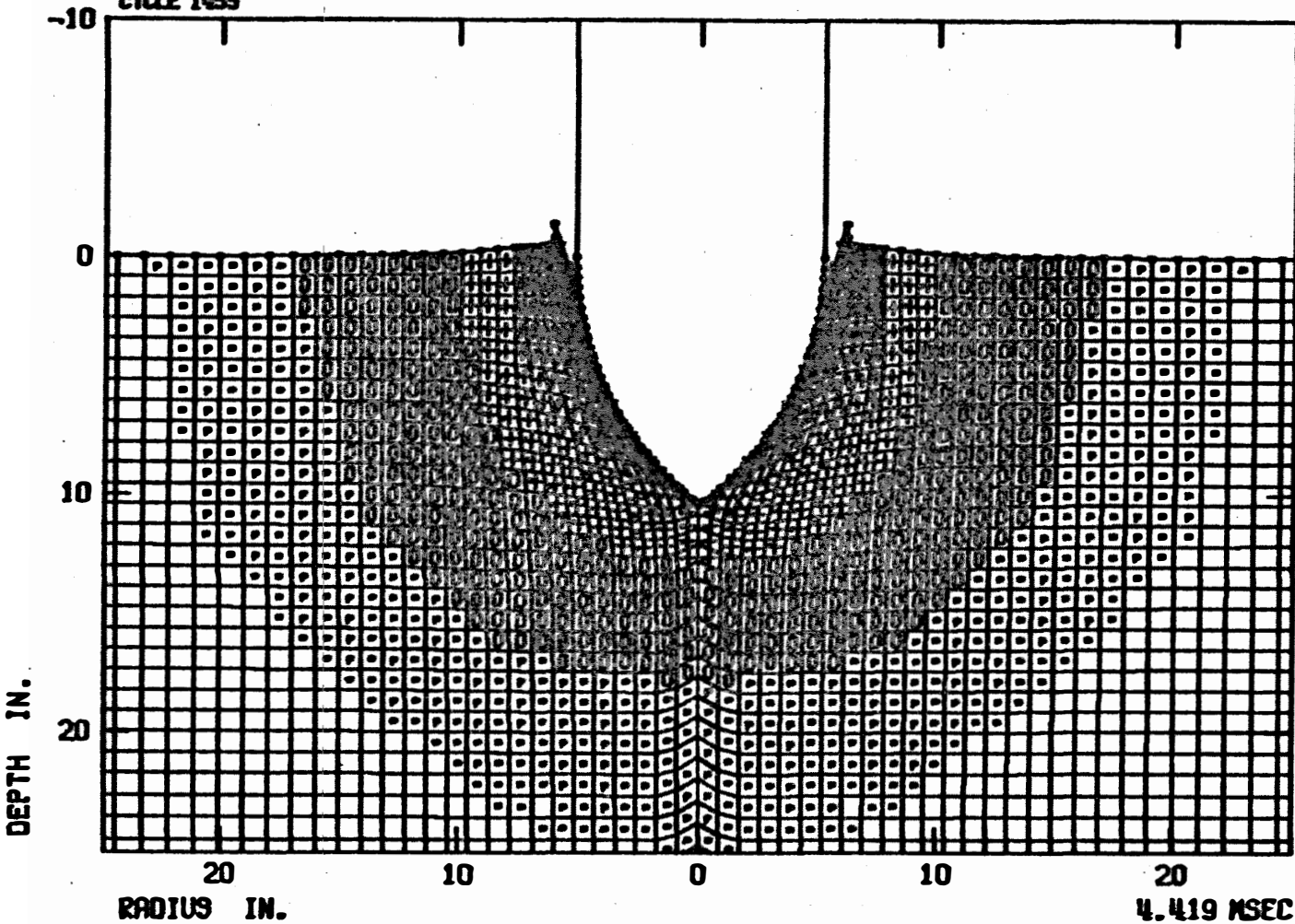


Figure 12. Grid Configuration and Generalized Plastic Strain Field
at $6\sqrt{3}$ -in. Penetration Depth, Case 3.

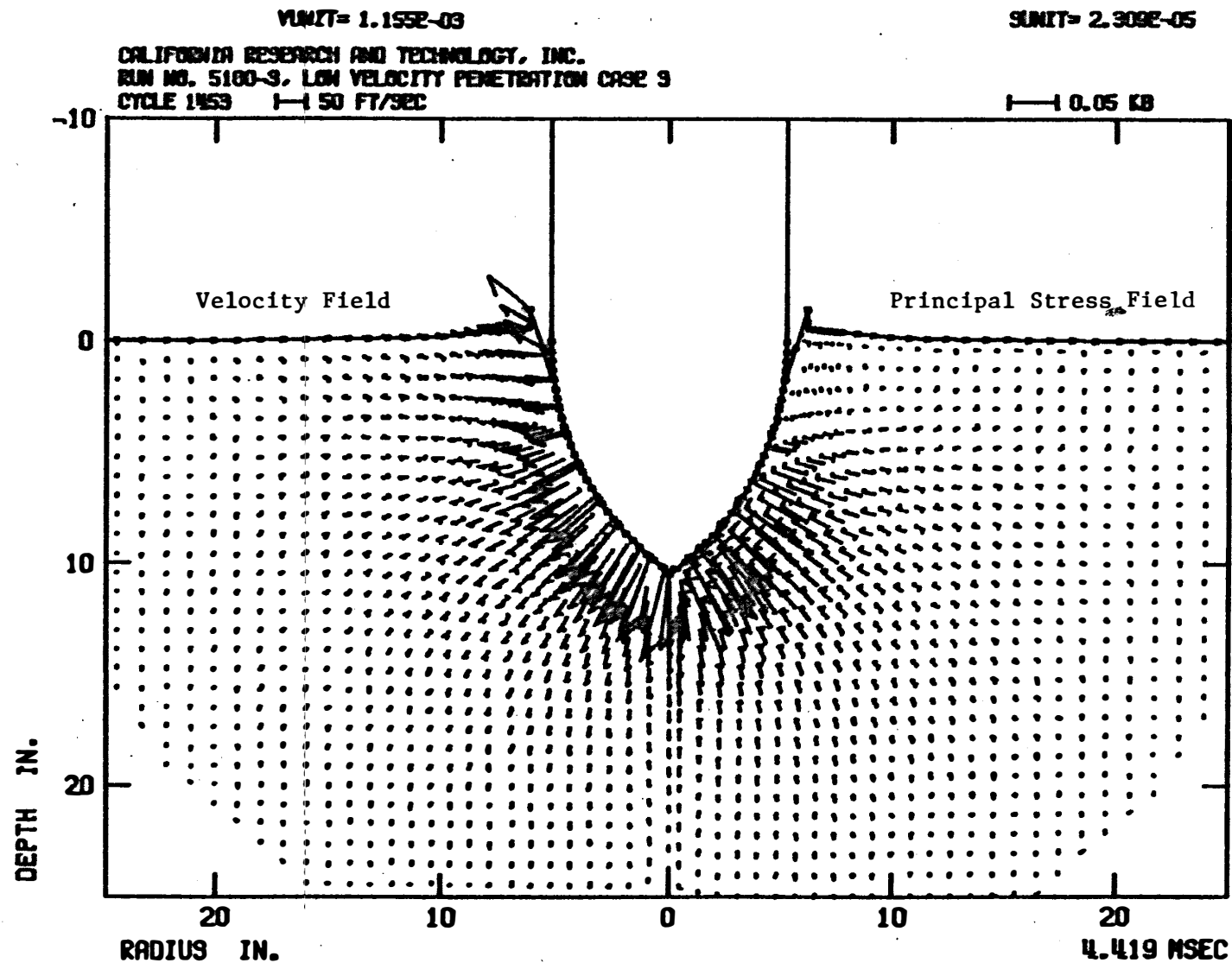


Figure 13. Velocity Field and Principal Stress Field at $6\sqrt{3}$ -in. Penetration Depth, Case 3.

CALIFORNIA RESEARCH AND TECHNOLOGY, INC.
RUN NO. 5180-3, LOW VELOCITY PENETRATION CASE 3
CYCLE 2221

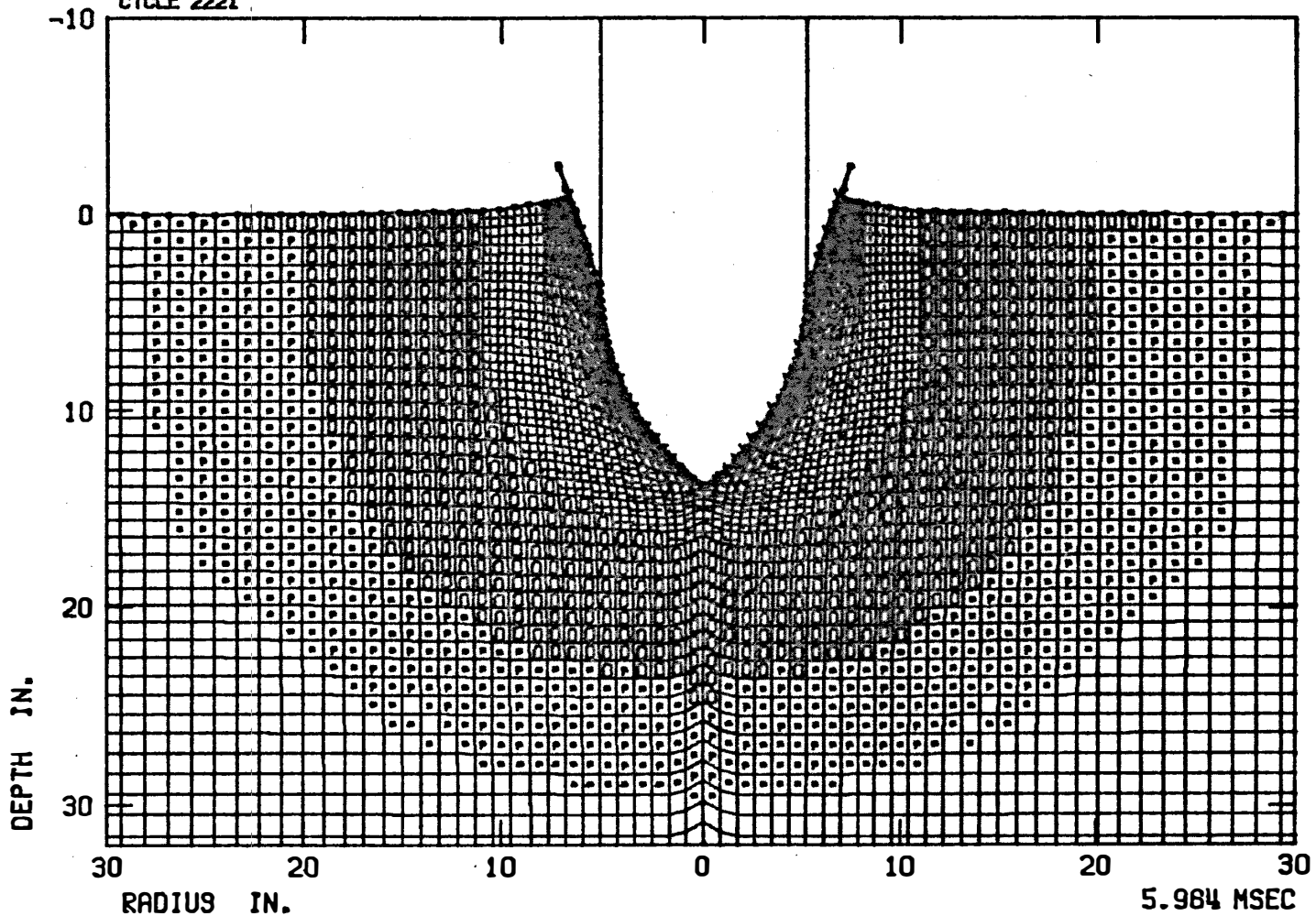


Figure 14. Grid Configuration and Generalized Plastic Strain Field
at $8\sqrt{3}$ -in. Penetration Depth, Case 3.

VUNIT= 1.155E-03

SUNIT= 2.309E-05

CALIFORNIA RESEARCH AND TECHNOLOGY, INC.
RUN NO. 5180-3. LOW VELOCITY PENETRATION CASE 3
CYCLE 2221 $\downarrow \rightarrow$ 100 FT/SEC

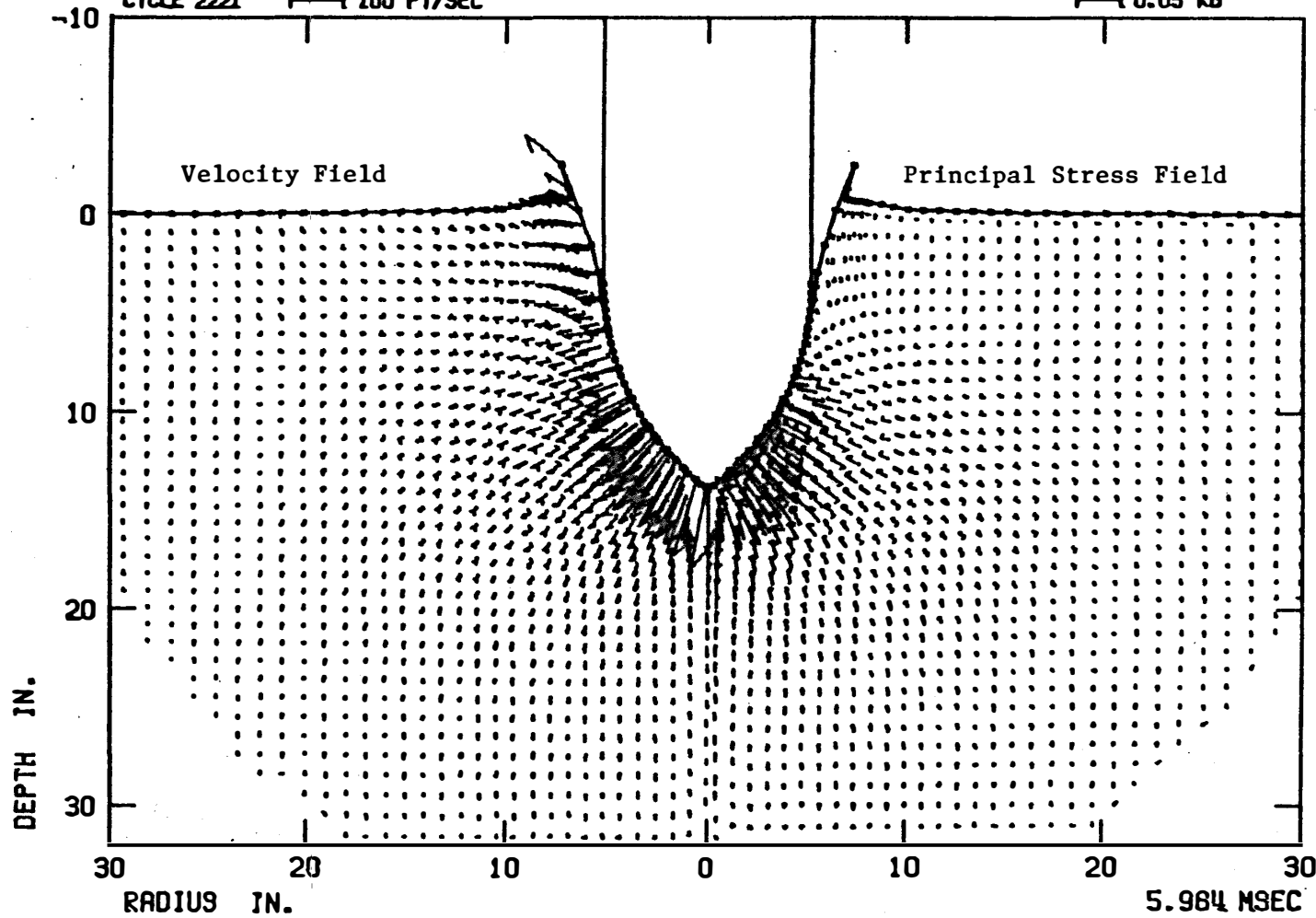


Figure 15. Velocity Field and Principal Stress Field
at $8\sqrt{3}$ -in. Penetration Depth, Case 3.

CALIFORNIA RESEARCH AND TECHNOLOGY, INC.
LOW VELOCITY PENETRATION AT $2\sqrt{3}$ INCHES

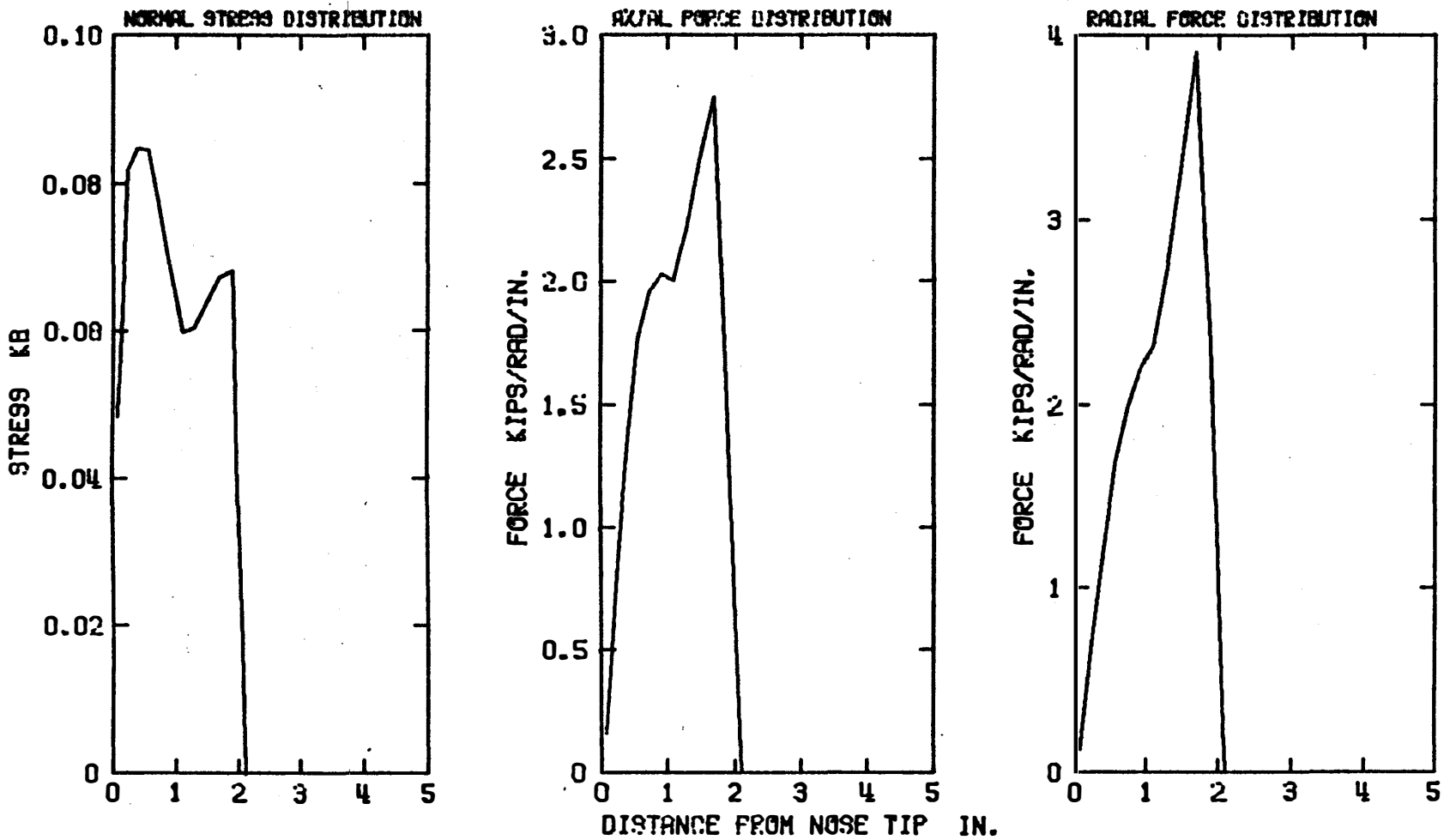


Figure 16. Penetrator Loading Distributions at $2\sqrt{3}$ -in. Penetration Depth, Case 3.

CALIFORNIA RESEARCH AND TECHNOLOGY, INC.
LOW VELOCITY PENETRATION AT $4\sqrt{3}$ INCHES

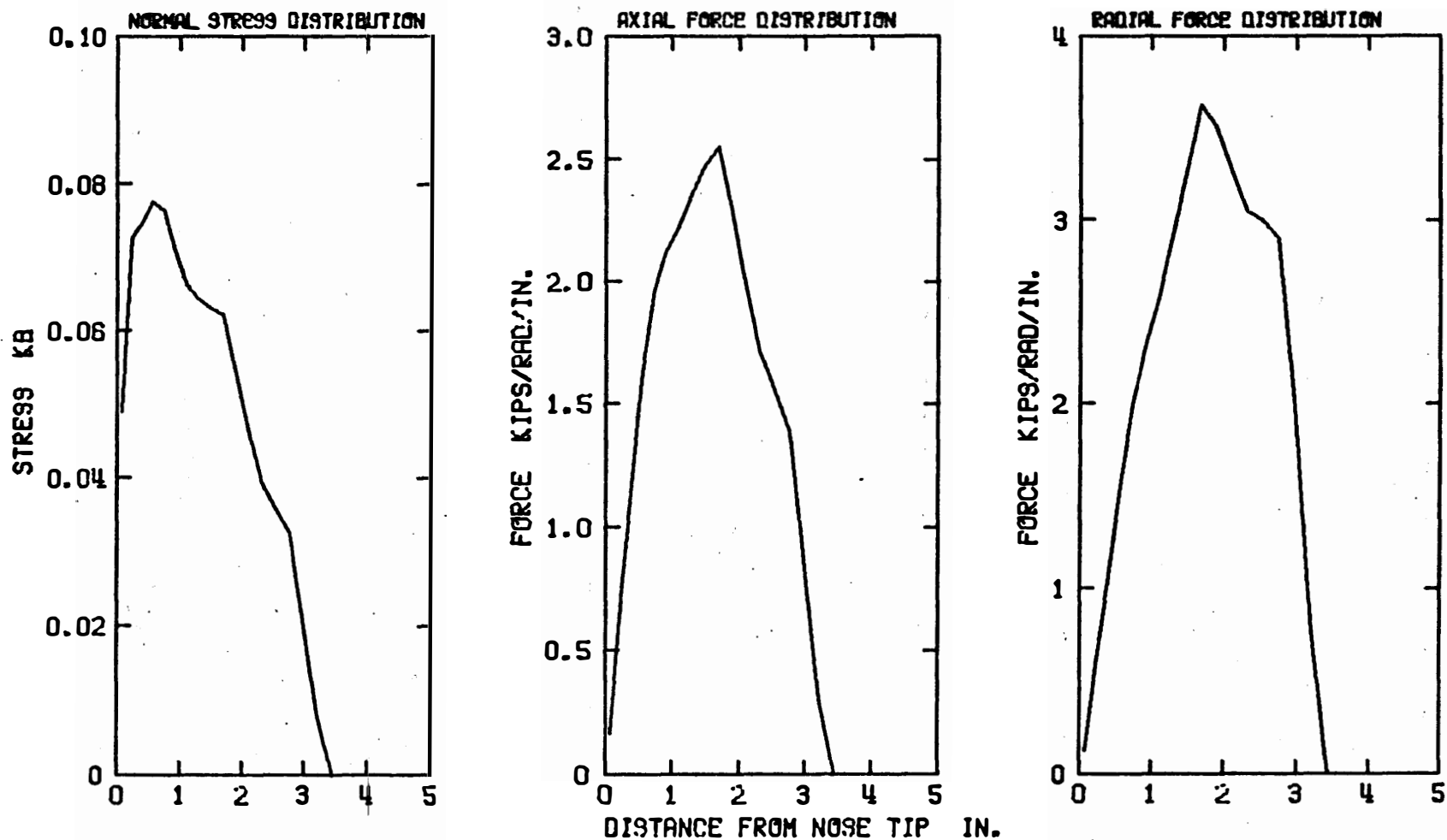


Figure 17. Penetrator Loading Distributions at $4\sqrt{3}$ -in. Penetration Depth, Case 3.

CALIFORNIA RESEARCH AND TECHNOLOGY, INC.
LOW VELOCITY PENETRATION AT $6\sqrt{3}$ INCHES

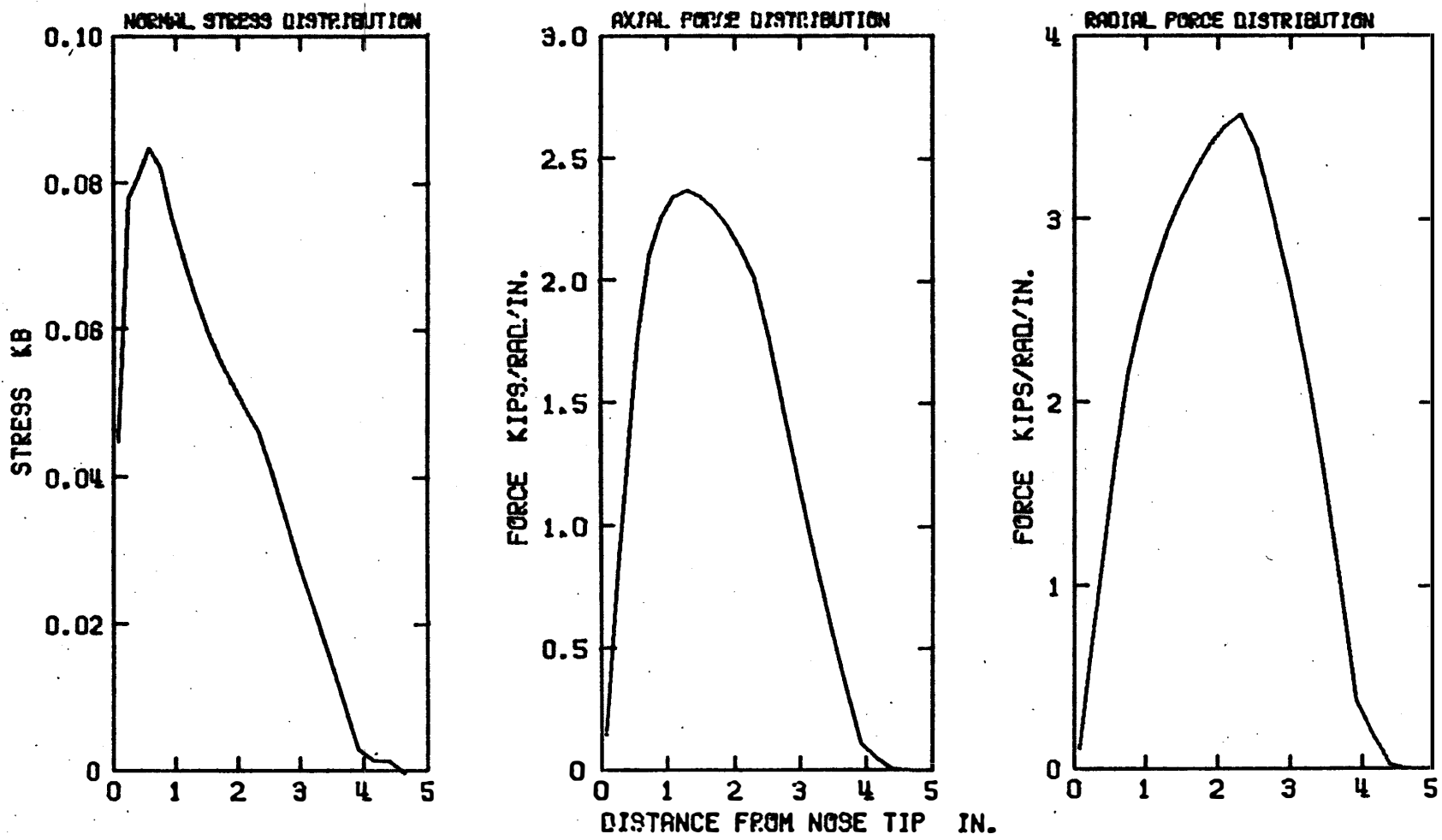


Figure 18. Penetrator Loading Distributions at $6\sqrt{3}$ -in. Penetration Depth, Case 3.

CALIFORNIA RESEARCH AND TECHNOLOGY, INC.
LOW VELOCITY PENETRATION AT $8\sqrt{3}$ INCHES

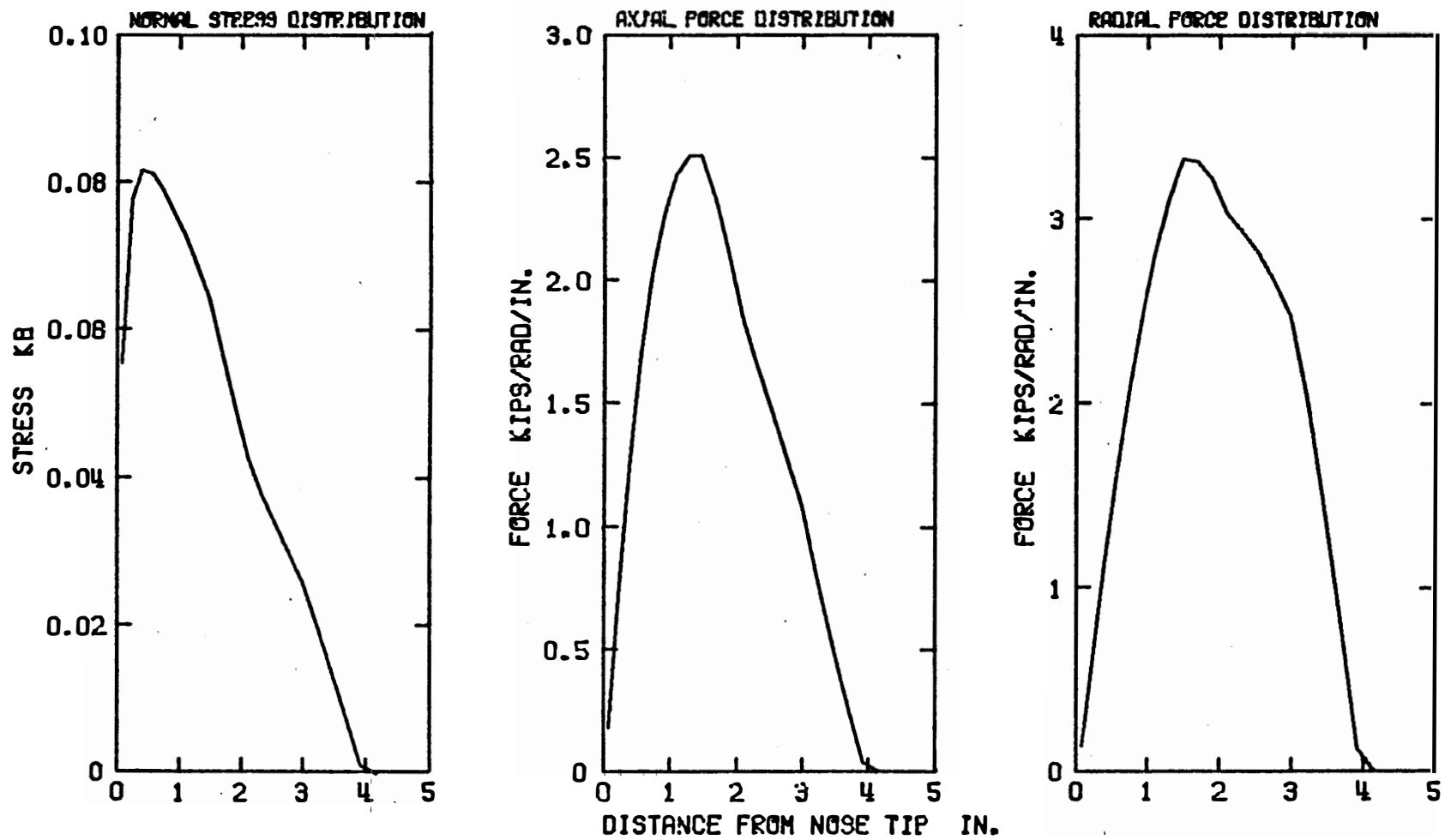


Figure 19. Penetrator Loading Distributions at $8\sqrt{3}$ -in. Penetration Depth, Case 3.